





Virtual screening and molecular dynamics simulation study of plant-derived compounds to identify potential inhibitors of main protease from SARS-CoV-2

Shafi Mahmud, Mohammad Abu Raihan Uddin , Gobindo Kumar Paul, Mst. Sharmin Sultana Shimu, Saiful Islam, Ekhtiar Rahman, Ariful Islam, Md. Samiul Islam , Maria Meha Promi, Talha Bin Emran  and Md. Abu Saleh 

Corresponding author: Md. Abu Saleh, Department of Genetic Engineering and Biotechnology, University of Rajshahi, Administration Building 1, Rajshahi 6205, Bangladesh. Tel: +8801716731747; Fax: +88 0721750064; E-mail: saleh@ru.ac.bd

Abstract

The new coronavirus (SARS-CoV-2) halts the world economy and caused unbearable medical emergency due to high transmission rate and also no effective vaccine and drugs has been developed which brought the world pandemic situations. The main protease (M^{PTO}) of SARS-CoV-2 may act as an effective target for drug development due to the conservation level. Herein, we have employed a rigorous literature review pipeline to enlist 3063 compounds from more than 200 plants from the Asian region. Therefore, the virtual screening procedure helps us to shortlist the total compounds into 19 based on their better binding energy. Moreover, the Prime MM-GBSA procedure screened the compound dataset further where curcumin, gartanin and robinetin had a score of (−59.439, −52.421 and −47.544) kcal/mol, respectively. The

Shafi Mahmud is an MS student in Genetic Engineering and Biotechnology at the University of Rajshahi, Bangladesh. He has received a BSc degree from the same university. He also serves as campus Ambassador of Boi-Bio-1, Bioinformatics Research Foundation, Bangladesh. He has expertise in molecular modeling, docking, medicinal chemistry and dynamics simulation.

Mohammad Abu Raihan Uddin is a graduate student at the Department of Biochemistry and Biotechnology, University of Science and Technology Chittagong. His research interest lies in bioinformatics, computational biology, computer-aided drug design and immune-informatics.

Gobindo Kumar Paul is an MS student in the Department of Genetic Engineering and Biotechnology at the University of Rajshahi, Bangladesh. He has expertise in microbiology, environmental microbiology, plant physiology, medicinal chemistry, enzymology and bioinformatics.

Mst. Sharmin Sultana Shimu is a final year student at the Department of Genetic Engineering and Biotechnology, University of Rajshahi. Her research interests include medicinal chemistry, bioinformatics and protein modeling.

Saiful Islam is an undergraduate student at the Department of Biochemistry and Biotechnology, University of Science and Technology Chittagong. His research interests include bioinformatics, computer-aided drug design and development, immuno-informatics.

Ekhtiar Rahman is a graduate student in Genetic Engineering and Biotechnology at the University of Rajshahi. His research interests include molecular biology, computer-aided drug design, docking and molecular dynamics.

Ariful Islam is a graduate student at the Department of Genetic Engineering and Biotechnology, University of Rajshahi, Bangladesh. He is enthusiastic in research with molecular biotechnology, microbiology, bioinformatics and computational pharmacology.

Md. Samiul Islam is a Ph.D. fellow at the Department of Molecular Plant Pathology, Huazhong Agricultural University, Wuhan, China. He is currently working as a laboratory consultant at the COVID-19 RT-PCR Laboratory of Rangpur Medical College, Bangladesh. His PhD research focuses on resistant gene isolation, purification, peptide prediction, functional genomics and drug design.

Maria Meha Promi is an undergraduate student in Genetic Engineering and Biotechnology at the University of Rajshahi. His research interests include molecular biology, computer-aided drug design, docking and molecular dynamics.

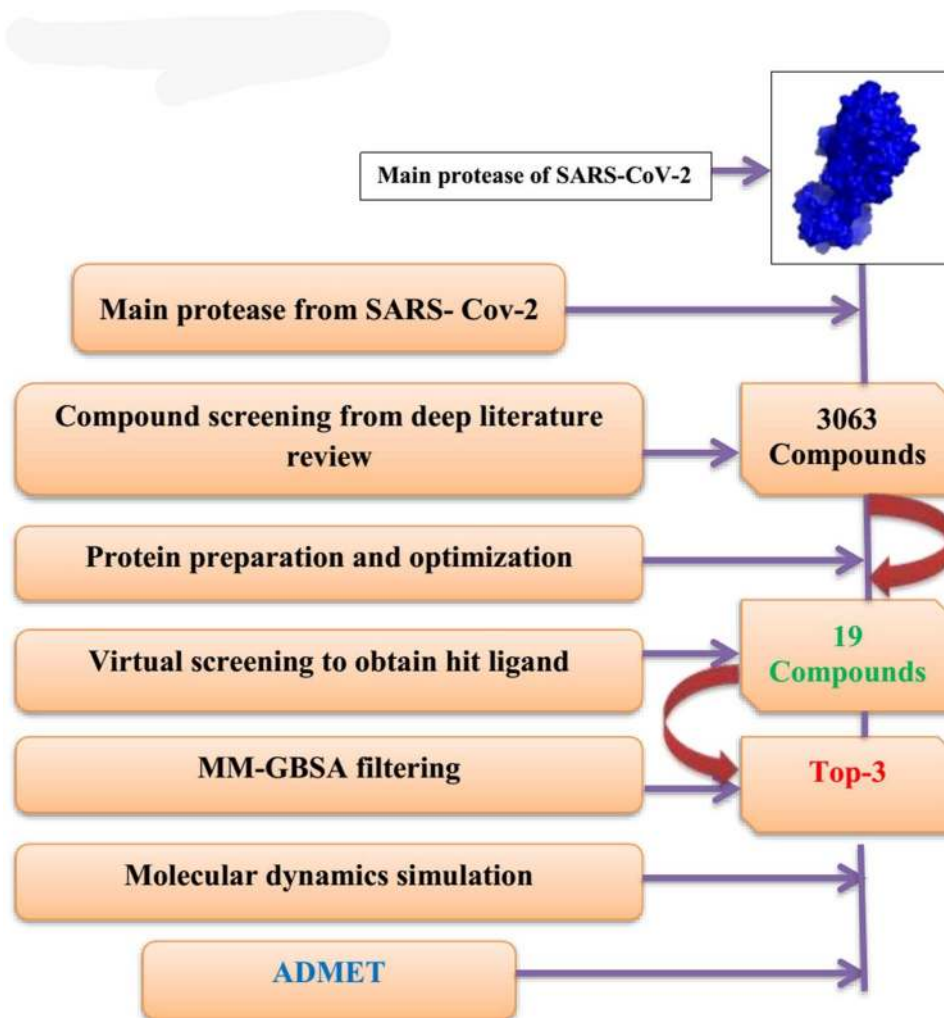
Talha Bin Emran has been working as an Assistant Professor in the Department of Pharmacy at the BGC Trust University, Bangladesh. Dr. Emran received his B.Sc. and MS in Biochemistry from the University of Chittagong, PhD from Graduate School of Medicines, Kanazawa University, Japan. His research work focuses on medicinal chemistry, computer-aided drug design, bioinformatics, molecular docking and dynamics simulation.

Md. Abu Saleh is an Associate Professor in the Department of Genetic Engineering and Biotechnology, University of Rajshahi. He received the PhD degree in enzymology and enzyme kinetics from CAS, China. His research focuses on microbiology, enzymology, medicinal chemistry, bioinformatics and protein modeling.

Submitted: 17 October 2020; Received (in revised form): 9 December 2020

top three ligands based on binding energy and MM-GBSA scores have most of the binding in the catalytic groove Cys145, His41, Met165, required for the target protein inhibition. The molecular dynamics simulation study confirms the docked complex rigidity and stability by exploring root mean square deviations, root mean square fluctuations, solvent accessible surface area, radius of gyration and hydrogen bond analysis from simulation trajectories. The post-molecular dynamics analysis also confirms the interactions of the curcumin, gartanin and robinetin in the similar binding pockets. Our computational drug designing approach may contribute to the development of drugs against SARS-CoV-2.

Graphical Abstract



Key words: COVID-19; SARS-CoV-2; Virtual screening; MM-GBSA; ADMET; Molecular dynamics

Introduction

The world is currently facing a miserable situation due to the outbreak of the COVID-19 (coronavirus diseases 2019) viral pandemic which occurred by a novel coronavirus namely SARS-CoV-2 (severe acute respiratory syndrome coronavirus-2) [1]. Since the appearance of the first confirmed case in late December of 2019 at Wuhan, capital of Central China's Hubei Province [2], this viral pneumonia has infected 35 659 007 people with 1 044 269 confirmed dead till 7 October 2020 [3]. Due to the pandemic, most of the countries were forced to adopt a lockdown mode along with social distancing and quarantine strategy triggering dilapidated economic fallout and human suffering [4]. This

SARS-CoV-2 is a genus of beta (β)-coronavirus, which enveloped with a single-stranded RNA virus [5]. Six types of coronaviruses are pathogenic in the human body, most of them including, HCoV-229E, HCoV-HKU1, HCoVNL63 and HCoV-OC43 are less pathogenic and responsible for causing the common cold, but in China and Saudi Arabia, the severe infectious SARS-CoV and MERS-CoV have shown higher pathogenicity in the year of 2002 and 2012. The case fatality rate was relatively higher the SARS (~10%) and MERS (~35%) than COVID-19 (0.2–7.7%) [6] where its basic reproduction number (R_0) (~5.7) of COVID-19 [7] is higher compared to the SARS (~2–3) and MERS (<1) [8]. The SARS-CoV-2 genome has 79% similarity with SARS-CoV-1 and 50% with MERS-CoV [9], which declared a successor of SARS-CoV-1 by

the U.S. National Institutes of Health [10]. The genomic RNA of Coronaviruses ranges from 26–32 kb containing a minimum of six open reading frames [8] and two overlapping polyproteins (pp1a and pp1ab) are encoded by the first ORF (ORF1a/b) of its two-thirds of the genome length [11].

The main protease (M^{pro}) also is known as 3CL pro (3-chymotrypsin-like cysteine protease CCP), which along with the aid of papain-like protease (PL pro) proteolytically cleaves these viral polyproteins into 16 non-structural proteins (nsp1-16) [12]. The M^{pro} cleaves polypeptide sequence after glutamate residues which makes it an ideal candidate due to its substrate specificity [8]. The polyprotein cleavage sites for M^{pro} in MERS-CoV, SARS-CoV, SARS-CoV-2 also exhibit similar kinds of substrate specificity and recognition [13]. This is a vital step in the interim of viral replication; the enzymes like RdRp-(RNA dependent RNA polymerase) or nsp13 are essential for the replication process, but it cannot fully function without prior photolytic release [8]. These above-mentioned non-structural proteins enjoy the production of sub-genomic RNAs that eventually translated into an envelope, membrane, spike and nucleocapsid proteins as well as other accessory proteins [11].

Active SARS-CoV-2 M^{pro} is a cysteine protease homodimer that combines two protomers stationing nearly perpendicular to one another [11]. Each one of the protomers contains three domains, and features a substrate-binding noncanonical catalytic dyad (His41 and Cys145) that is located in a cleft within domains I and II (residues 10–99 and 100–182, respectively) [14]. Domains I and II consist of chymotrypsin (which like double β -barrel fold), whereas domain III (198–303 amino acid residues) is mainly comprised of five antiparallel α -helices [12]. The M^{pro} is conserved among coronaviruses [11]. It shows ~99% identity with BatCoV RaTG13 M^{pro} , ~96% with the previous SARS-CoV M^{pro} and ~50% only with MERS-CoV M^{pro} through amino acid sequence alignment [8], in contrast, SARS-CoV-2 M^{pro} plays a pivotal role in arbitrating viral replication and transcription, and inhibition of its activity is expected to block the viral replication, and maturation by providing a key enzyme [11]. SARS-CoV-2 M^{pro} has a particular cleavage specificity unlike any other human proteases [5]. Therefore, this enzyme is an attractive therapeutic target for CoVs than others [8].

Moreover, synthesis and design of new antiviral drugs can be aided through plant-based phytochemicals with more efficacy and specificity. For example, isoquinoline types alkaloid, emetine is widely used as an amoebicidal drug, quinone as well as cancer drug paclitaxel [15, 16]. From the early 1980s to till the day, most drug candidates developed from plant-based natural compounds [17]. Moreover, the use of traditional Chinese medicine Chongqing, in Chinese COVID-19 patients, suggests that plant-based drug molecules can act as an effective solution as complementary or addition with therapeutic drugs [18]. Furthermore, effective and greater antiviral activity was observed for numerous plant-derived compounds, for example, SARS [19], SARS-CoV-2 [20] and Chikungunya [21].

Computer-aided drug design would be a great weapon in this regard [22]. It is an efficient tool in the searching tool for promising drug candidates in a very short time and cost-effective way [23]. Here an in-depth literature review was done to make a library of plant-derived natural compounds from commonly used medicinal plants in the Asian region. We further used a virtual screening technique to shortlist the potent phytochemicals with inhibiting the activity of SARS-CoV-2 M^{pro} . Top hit molecules derived from these were then docked against the target enzyme. A molecular dynamics study was preferred due to the lack of reliance on providing the precise binding

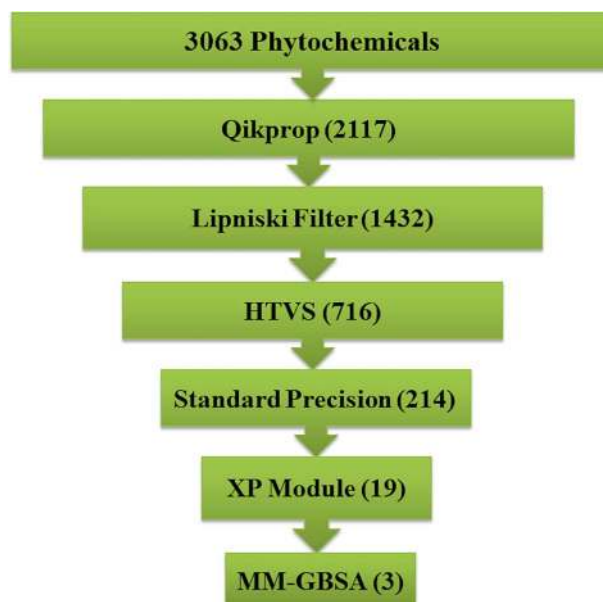


Figure 1. The virtual screening workflow in Schrodinger where three lead molecules were screened.

mode, binding energy, entropy energy, constant motion effect and solvation effect through molecular docking [24]. We propose that these compounds could be further potential therapeutic candidates for *in vitro* and *in vivo* antiviral studies followed by a clinical trial of SARS-CoV-2.

Methods and materials

Protein preparation and grid generation

The three-dimensional structure of the M^{pro} enzyme of SARS-CoV-2 (PDB ID: 6LU7) [25] was taken from the protein data bank [26]. Protein preparation wizard of the Schrödinger suite version 2020-3 was subjected for preparation [27]. The water molecules were removed beyond 5.0 Å from het groups. The protein structure was preprocessed by adding the hydrogen with assigned bond orders and creating disulfide bonds, including the conversion of selenomethionines to methionines whereby it is applicable. H-bond networks were optimized, and protonation states were yields at pH 7.0. Finally, by applying the OPLS3e force field, the energy minimization process was done [28]. Afterward, keeping the active site residues His41 and Cys145 specific as centroid the grid was generated using the 'Receptor Grid Generation' of the Schrödinger suite.

Ligand preparation

By literature search, about 3063 compounds (Supplementary file 1) were enlisted from the plant-based phytochemicals. The PubChem database [29] was utilized for compound extraction and the Ligprep module of the Schrödinger suite [30] was employed by applying default parameters for ligand molecule preparation. Furthermore, Epik version v5.3 was used to obtain multiple states of the ligand molecules at pH 7.0 \pm 2, and for the likelihood of reliability in the biological condition, the high energy ionization/tautomer states were removed [31, 32]. The Qikprop version 6.5 program was run [33] before employing structure-based virtual screening, to screen the plant compounds by applying Lipinski's rules of five [34].

Table 1. Docking result (kcal/mol) and binding affinity (kcal/mol) estimation of the top 19 compounds

PubChem CID	Glide ligand efficiency	XP GScore	Glide evdw	Glide ecoul	Glide energy	Glide emodel	MM-GBSA ΔG Bind
Quercetin	-0.404	-8.916	-33.982	-8.344	-42.327	-55.652	-40.392
Myricetin	-0.365	-8.439	-36.917	-7.316	-44.228	-54.131	-46.958
Taxifolin	-0.356	-7.861	-36.554	-7.974	-44.528	-53.124	-41.944
Trans-Caftaric acid	-0.355	-7.812	-24.284	-15.667	-39.951	-52.398	-29.223
Luteolin	-0.353	-7.769	-30.199	-9.005	-39.204	-47.714	-42.913
7-methyl ether							
Curcumin	-0.287	-8.089	-38.839	-11.873	-50.713	-65.599	-59.439
Eriodictyol	-0.368	-7.759	-33.828	-6.779	-40.607	-57.201	-38.618
Gartanin	-0.265	-7.739	-40.519	-5.393	-45.912	-57.345	-52.421
3,4,5,3-Tetrahydroxybenzophenone	-0.426	-7.707	-29.861	-8.295	-38.157	-47.827	-42.163
Morin	-0.345	-7.852	-34.803	-5.631	-40.434	-52.9	-34.341
Lupiwighteone	-0.304	-7.601	-37.628	-5.556	-43.184	-53.094	-40.707
Leucopelargonidin	-0.361	-7.588	-35.143	-5.469	-40.612	-53.754	-39.133
Urolithin M5	-0.379	-7.687	-30.451	-5.541	-35.992	-48.645	-39.984
Licoflavonol	-0.292	-7.596	-35.035	-7.375	-42.409	-57.415	-42.745
3-O-Methylelagic acid	-0.326	-7.526	-33.089	-6.275	-39.364	-52.175	-46.258
Kaempferol	-0.356	-7.505	-33.638	-7.439	-41.077	-52.278	-38.735
Fisetin	-0.353	-7.449	-37.102	-6.207	-43.309	-54.449	-41.293
Luteolin	-0.353	-7.456	-37.321	-6.792	-44.113	-53.91	-39.487
Robinetin	-0.337	-7.452	-38.036	-5.358	-43.394	-55.424	-47.544

Virtual screening

The Glide program and its virtual screening workflow process were applied, including three docking protocols; high throughput virtual screening or HTVS, Standard Precision or SP module, and Extra Precision or XP module [35, 36]. To obtain the best compounds, we follow the previous literature as earlier published [37]. The HTVS was used to dock each ligand to the receptor, which generates one pose. Though the SP docking protocol provides a good scoring function retaining the good scoring states [38], about 50% of the total plant-derived compounds were transferred from HTVS to SP which helps to find out the false-positive results. Moreover, about 30% of SPs total ligand molecules were processed to XP, where the XP provides the best scoring states [35, 36]. Three poses for each ligand were generated by the XP.

Molecular mechanics-generalized born surface area (MM-GBSA)

Furthermore, only 10% of total compounds were specified postprocessed through MM-GBSA (molecular mechanics-generalized born surface area) for the accuracy of pose ranking and final selectivity [22, 39]. The Prime MM-GBSA module from the Schrodinger software package was utilized to calculate the binding affinity. The higher degree of rigidity of the ligand attached protein is indicated by the higher negative MM-GBSA value. The Prime MM-GBSA process consists of three different approaches: OPLS molecular mechanics energies, an SGB solvation model and a non-polar solvent. The binding free energies were calculated from the following equations:

$$\Delta G_{\text{bind}} = G_{\text{complex}} - (G_{\text{protein}} + G_{\text{ligand}}),$$

$$\text{where } G = \text{EMM} + \text{VSGB} + \text{GNP}$$

Therefore, to perceive their rigidity along with motion and structural stability in simulation conditions, the best three ligands are selected for further processing.

ADMET

The pharmacological and carcinogenic properties of the compounds were assessed with the aid of admetSAR [40], Swissadme [41] and PkCSM [42] webserver. The canonical smiles of the screened complex were used as an entry system of the complex.

Molecular dynamics simulation

The dynamics simulation of the screened ligand molecules was conducted to analyze the conformational behavior and protein stability of the complex. The YASARA software package version 20.1.1 [43] was used to conduct simulation for three complexes where the AMBER14 force field was used [44]. The NPT ensemble method was used in this simulation system and also, the Berendsen thermostat method was applied to control the temperature of the systems. To calculate long-range electrostatic interactions, the particle-mesh Ewald method [45] was employed, whereas a cut-off radius of 8 Å was considered [46] for short-range van der Waals and Coulomb interactions. The cubic cell, which was employed for simulation was 20 Å bigger than the drug-protein complexes in all cases and a periodic boundary condition was maintained. The system was neutralized by the addition of 0.9% NaCl at 298 K temperature. The initial energy minimization process of the systems was incorporated by the simulated annealing method by applying the steepest gradient algorithms [47]. The simulation was carried out with a time step of 1.25 fs and the simulation trajectory was saved for every 100 ps. Finally, the molecular dynamics simulation was carried out for 50 ns, and

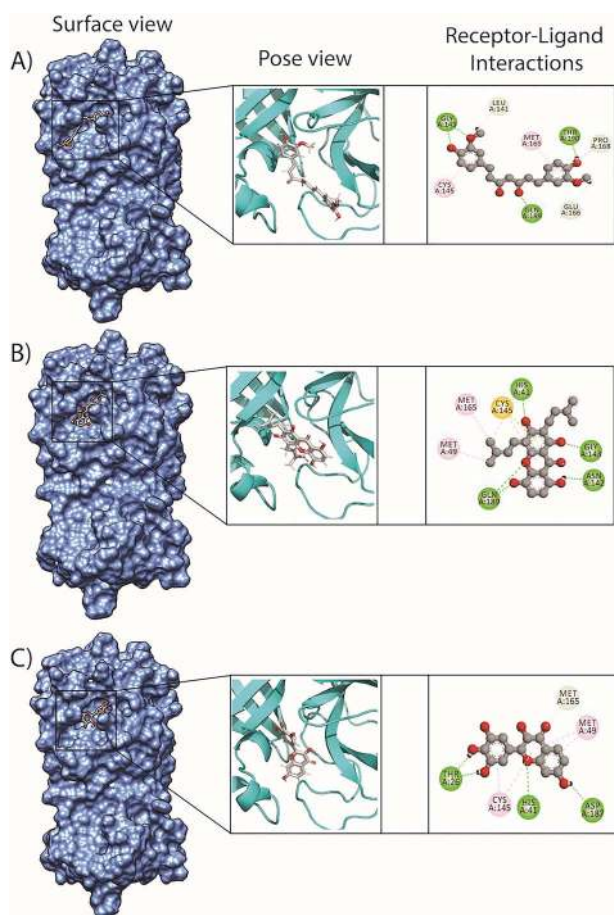


Figure 2. The non-bonded interaction of the top three docked complexes, where, A, B and C indicates the interaction diagram of Curcumin, Gartanin and Robinetin, respectively. The figures were obtained through Discovery Studio version 4.5.0., Chimera version 1.14 and Pymol software version 2.4.0 package.

trajectories were used to analyze root mean square deviations (RMSD), root mean square fluctuations (RMSF), solvent accessible surface area (SASA), radius of gyration (Rg), and hydrogen bond number of the system [22, 48, 49].

Results

Molecular docking analysis

The result of virtual screening revealed the identification of about three compounds as a potential inhibitor as they exhibit non-covalent interactions with the amino acid derived from the catalytic residue of the M^{Pro} of SARS-CoV-2. The large phytochemical dataset was initially screened in Qikprop module where 2117 compounds were passed to the next passed, following Lipinski filtering where 1432 compounds were screened. The high throughput virtual screening module then filter and 716 phytochemicals were again filtered in SP or standard precision program. The XP or extra precision program was allowed for more accurate screening (Figure 1). The glide ligand efficiency score, SP GScore, Glide evdw, Glide ecoul, Glide energy, Glide emodel score were taken into consideration for screening the ligand molecules from the dataset. The lower energy score from these descriptors utilized to rank the top 19 molecules from the dataset. The XP Gscore was found higher in Quercetin as

Table 2. Non-bond interaction between top three compounds and SARS-CoV-2 M^{Pro}

PubChem CID	Residue in contact	Interaction types	Distance in Å
Curcumin	GLY143	Conventional hydrogen bond	2.2
	GLY143	Conventional hydrogen bond	2.31
	GLN189	Conventional hydrogen bond	1.89
	THR190	Conventional hydrogen bond	1.67
	PRO168	Carbon hydrogen bond	2.47
	LEU141	Carbon hydrogen bond	2.46
	GLU166	Carbon hydrogen bond	2.68
	CYS145	Pi-Alkyl	4.18
	MET165	Pi-Alkyl	4.87
	PRO168	Pi-Alkyl	5.42
Gartanin	HIS41	Conventional hydrogen bond	1.97
	GLY143	Conventional hydrogen bond	2.06
	GLN189	Conventional hydrogen bond	2.64
	GLN189	Conventional hydrogen bond	2.64
	ASN142	Conventional hydrogen bond	2.66
	ASN142	Carbon hydrogen bond	2.38
	CYS145	Pi-Sulfur	4.17
	MET49	Alkyl	4.31
	MET165	Alkyl	4.23
	HIS41	Pi-Alkyl	4.36
Robinetin	CYS145	Pi-Alkyl	5.28
	HIS41	Conventional hydrogen bond	3.05
	THR26	Conventional hydrogen bond	1.85
	ASP187	Conventional hydrogen bond	2.72
	THR26	Conventional hydrogen bond	1.78
	MET165	Carbon hydrogen bond	2.59
	MET49	Pi-Alkyl	5.21
	CYS145	Pi-Alkyl	5.08
	MET49	Pi-Alkyl	4.49
	CYS145	Pi-Alkyl	4.79

–8.916Kcal/mol, whereas Gartanin had a better affinity in Glide energy (–45.912 Kcal/mol).

Moreover, for better approximation, the poses of the ligand molecules generated from the XP module was additionally processed with MM-GBSA. Hence, among 19 compounds, only three compounds have been selected by observing the binding energy (ΔG_{bind}) with the catalytic region of the M^{Pro}. Although, quercetin, myrecetin, taxifolin, trans-caftaric acid, luteolin 7 methyl ether exhibit better energy score but they had higher energy score MM-GBSA. So these molecules were not taken

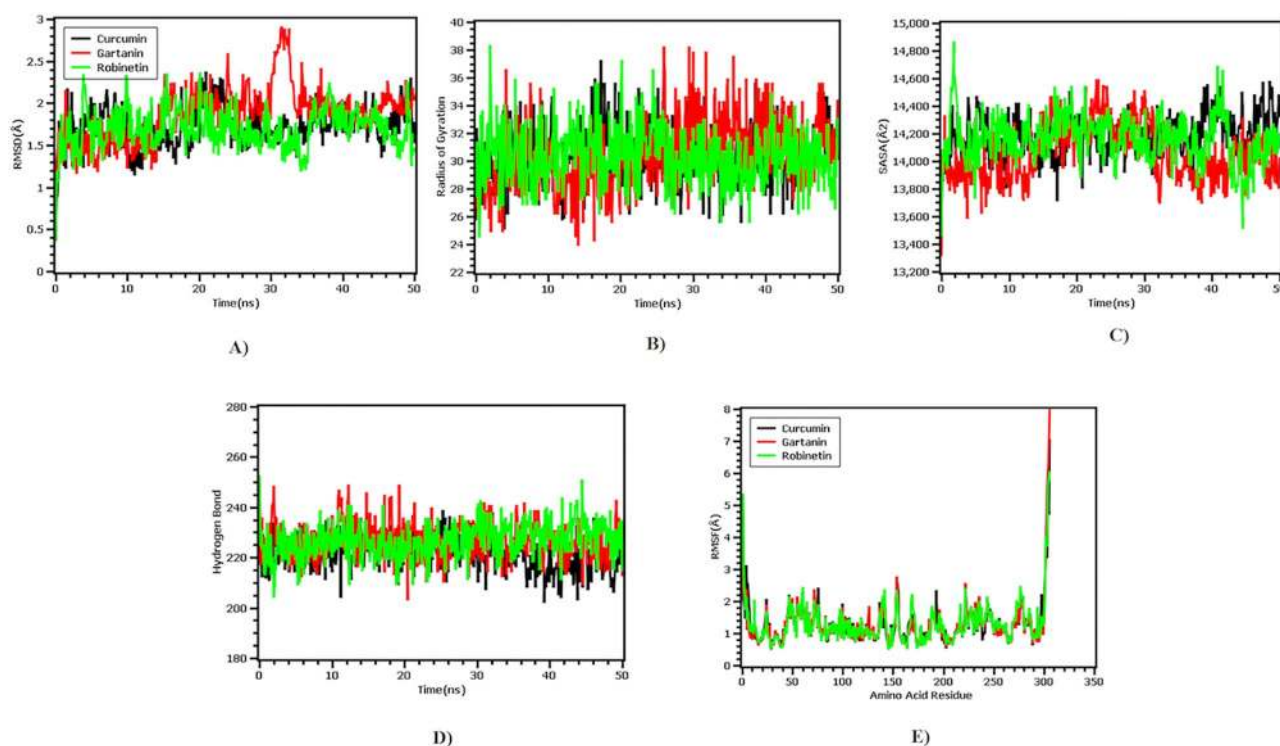


Figure 3. The molecular dynamics simulation of the docked three complex, here A, B, C, D, E indicates RMSD, Rg, SASA, hydrogen bond and root mean square fluctuation, respectively.

into the consideration as the top three complexes, including curcumin, gartanin and robinetin exhibited greater negative affinity in MM-GBSA threshold (-59.439 , -52.421 and -47.544) kcal/mol, respectively. The docking and binding energy results of 19 compounds are tabulated in Table 1, binding interaction in Figure 2 and the interacting residues of the M^{PTO} with ligand molecules with the active site residues are shown in Table 2.

ADMET

The pharmacokinetics and toxicity properties of the ligand need to be assessed to ensure the safety and efficacy level of the hit molecules. Moreover, CNS permeability, blood-brain barrier absorption, p-glycoprotein inhibition, hepatotoxicity, carcinogenicity, CYP inhibition of the lead molecules were checked. The CNS permeability determines the ability to permeable through the blood-brain barrier where $CNS > -2$ considered to penetrate the central nervous system. Among the three compounds, no carcinogenic and toxicity profiles were observed in carcinogenicity and AMES toxicity assessment. The selected compounds exhibit a positive response in Lipinski rule of five where the number of hydrogen bond donors, acceptor and surface area of the ligand molecules were explored. Also, the molecular weight (MW) of the compounds was (368.38, 396.439 and 302.238) g/mol, respectively, for curcumin, gartanin and robinetin which was good for heat molecules consideration as higher MW in compounds violates the rule of Lipinski. The hydrogen bond donors were found as 2, 4 and 5 whereas hydrogen bond acceptors were found as 6, 6 and 7, respectively, for curcumin, gartanin and robinetin. Although, some carcinogenic properties and the violation of Lipinski's rule of five was observed for some cancer drugs but some deviation in the ADMET properties might be acceptable if the drug molecules exhibit desired pharmacological properties Table 3.

Table 3. Pharmacological profile of the top three ligand molecules that were derived from admetSAR, Swissadme and pKCSM webserver

Parameter	Curcumin	Gartanin	Robinetin
CNS	-2.99	-1.993	-3.288
MW	368.38	396.439	302.238
SASA	156.532	167.208	122.108
Donor HB	2	4	5
Acceptor HB	6	6	7
Caco2 permeability	-0.093	0.252	-0.563
P-glycoprotein I inhibitor	Yes	Yes	No
P-glycoprotein II inhibitor	Yes	Yes	No
BBB permeability	-0.562	-1.224	-1.403
Hepatotoxicity	No	No	No
Carcinogenicity	0.7130	0.7457	0.6750
AMES toxicity	No	No	No
CYP2D6 substrate	No	No	No
CYP3A4 substrate	Yes	Yes	No
CYP1A2 inhibitor	Yes	No	Yes
CYP2C19 inhibitor	Yes	Yes	No
CYP2C9 inhibitor	Yes	Yes	No
CYP2D6 inhibitor	No	No	No
CYP3A4 inhibitor	Yes	No	No

CNS: central nervous system activity.

Molecular dynamics simulation

The molecular dynamics simulation of the docked complex was employed to validate the docking study, and also the dynamic motion of the docked complex was analyzed to understand their degree of stability. The RMSF of the c-alpha atoms is illustrated in Figure 3, where curcumin and M^{PTO} complex had initial stability and fluctuated a little bit after 10 ns. This complex maintained

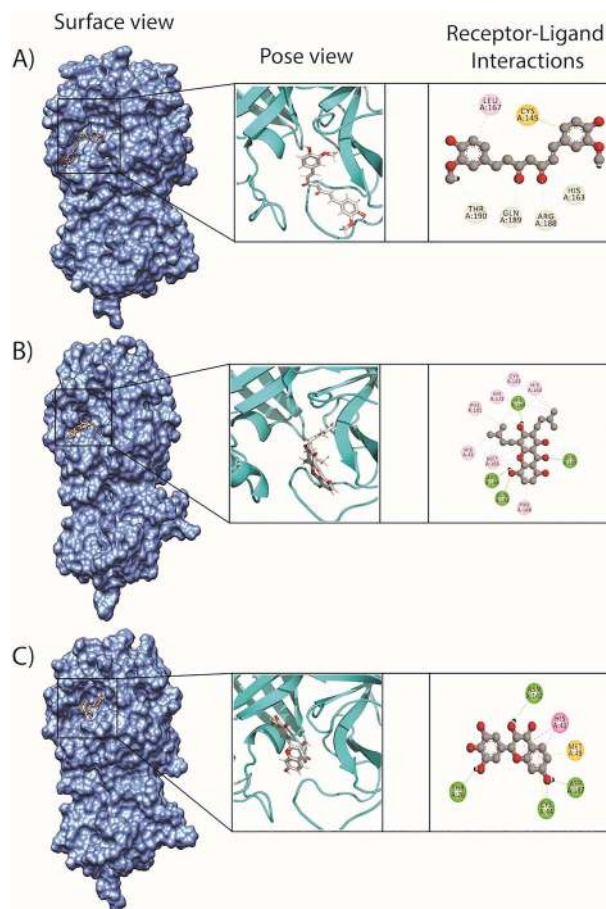
Table 4. Post-MD interaction analysis in the docked complexes, here key amino acid residues are present as like as pre-MD structure

Compound	Residue in contact	Interaction type	Distance in Å
Curcumin	Arg188	Hydrogen bond	2.98
	Gln189	Hydrogen bond	2.98
	His163	Hydrogen bond	2.87
	Thr190	Hydrogen bond	2.54
	Cys145	Pi-Sulfur	4.22
	Ala191	Alkyl	4.13
	His163	Pi-Alkyl	4.40
	Leu167	Pi-Alkyl	5.08
	Gartanin	Gln189	Hydrogen bond
Gln192		Hydrogen bond	2.33
His164		Hydrogen bond	1.97
Arg188		Hydrogen bond	1.77
Met165		Alkyl	4.95
Cys145		Alkyl	4.65
His41		Pi-alkyl	4.29
His163		Pi-Alkyl	4.08
His164		Pi-Alkyl	5.43
Phe181		Pi-Alkyl	4.25
Robinetin	Pro168	Pi-Alkyl	5.36
	Cys44	Hydrogen bond	1.89
	Asn142	Hydrogen bond	2.45
	Thr26	Hydrogen bond	2.05
	Asp187	Hydrogen bond	1.79
	Met49	Pi-Sulfur	3.59
	His41	Pi-Pi-Stacked	4.28

a stable RMSD profile till the rest simulation periods. Also, the M^{Pro} protein from SARS-CoV-2 and robinetin complex had a similar RMSD trend till 35 ns and thereafter increased a little bit but these complexes did not over-fluctuate which demonstrates rigid conformation. Therefore, gartanin and M^{Pro} complex had a sharp increase in 30–35 ns, followed by a lower trend like the starting phase. Interestingly, all three complexes did not disclose RMSD descriptors over 2.5 Å which validates the rigid conformation of the drug complexes.

From Figure 3, it was also observed that robinetin complex had a similar Rg profile from 0 to 25 ns and thereafter, decreased Rg descriptor which indicates the tight packaging system of the complex as the Rg of the drug complex indicates the compact nature of the protein. Moreover, the degree of protein folding and unfolding greatly depends on the value of the Rgs. Moreover, gartanin and the M^{Pro} complex had lower Rg profile from 0 to 25 ns and a higher rise of Rg was observed from 25 to 45 ns, which indicates loose packaging of the system. The curcumin complexes had a moderate Rg profile compared to the other two complexes, which illustrates the less mobile nature.

Moreover, the solvent-accessible surface area of the complexes was analyzed from the simulation trajectories to assess the complex volume change through the simulation trajectory. Figure 3 demonstrates that the gartanin complex had a lower SASA profile at the starting phase and thereafter increased the SASA descriptors, which indicate expansion in the protein surface area. Therefore, this complex truncated its volume by a significant degree for the rest of the simulation trajectory. Interestingly, robinetin and curcumin complexes had a similar SASA trend which is higher than gartanin although little fluctuations were observed from 35–40 ns simulation time.

**Figure 4.** The post-MD binding interaction of three screened small molecules by taking last snapshot from molecular dynamics simulation.

On the other hand, the hydrogen bond has a crucial role in contributing stability in drug-protein complex and molecular recognition. All three drug-protein complexes remained stable in the simulation trajectory which indicates the rigidity of the complexes (Figure 3). The flexibility among the amino acid residues can be illustrated through the root mean square fluctuation or RMSF profile. From Figure 3, it can be observed that most of the amino acid residues from three complex had lower flexibility as they did not have higher RMSF values except, Ser1(helix-strand), Gly2(helix-strand), Phe3(helix-strand), Lys12(helix-strand), Thr24(beta-turn), Glu47(beta-turn), Glu55(helix-strand), Ile59(helix-strand), Asn72(beta-turn), Asn142(beta-turn), Phe140(beta-turn), Tyr154(beta-turn), Ala193(gamma-turn), Gln189(gamma-turn), Arg222(beta-turn), Gln244(helix-strand), Arg279(helix-strand), Ser301(beta-turn), Gly302(beta-turn), Val303(beta-turn), Thr304(beta-turn), Phe305(beta-turn) and Gln306(beta-turn) residue.

The last snapshot from the molecular dynamics simulation trajectory was analyzed again to find out a change in interaction dynamics of the docked complex. The results were tabulated in Table 4, where several interactions (Figure 4) were observed the same as docked complex which includes less conformational variation along with structural compactness.

The curcumin and M^{Pro} of the SARS-CoV-2 structure were stabilized by four hydrogen bonds at Arg188, Gln189, His163 and Thr190. Among these four hydrogen bonds, Thr190 was present in the pre-MD structure and this hydrogen bonding at

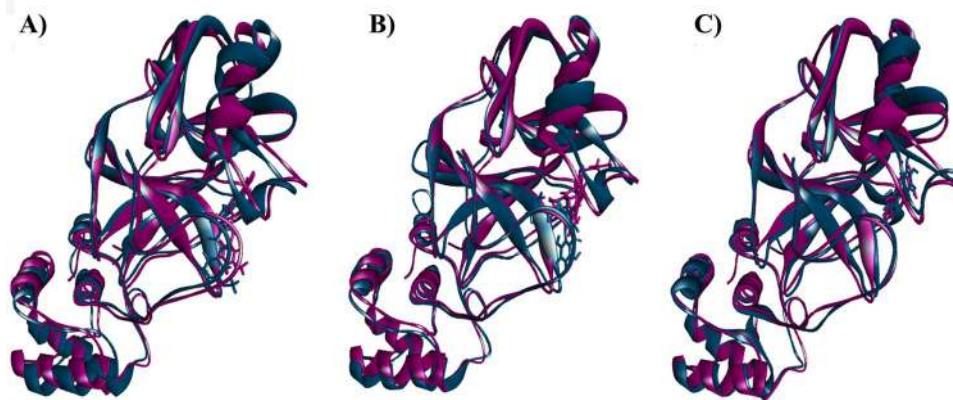


Figure 5. The superimposed drug-protein complex of pre- and post-MD structure. Here, purple color indicates pre-MD structure and dark blue indicates post-MD structure.

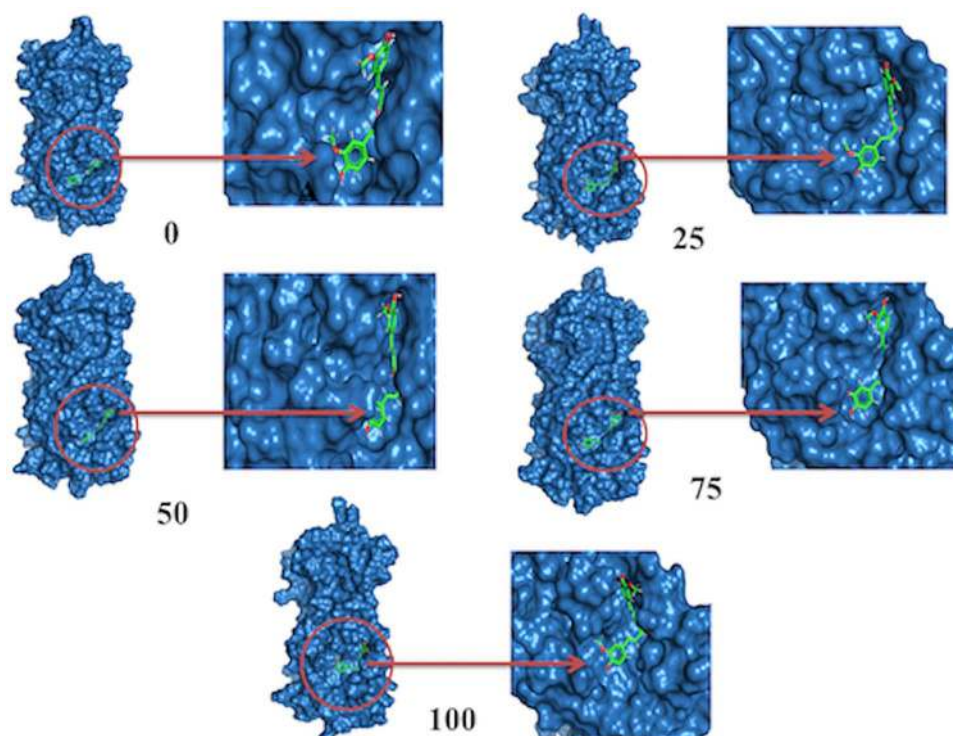


Figure 6. The surface view of the docked complex in molecular dynamics simulation. The snapshot was taken from 0, 25, 50, 75 and 100 ns, respectively, for Curcumin- M^{PTO} complex.

the active groove of the M^{PTO} enzyme may be responsible for favorable binding energy in docking. Moreover, one pi-sulfur bond at Cys145 (active site), one alkyl bond at Ala191 (active site), two pi-alkyl bonds at His163 (active site), Leu167 (active site) were also observed in post MD structure of the curcumin complex. Like curcumin, gartanin complex also had four hydrogen bonds but they are positioned among different residues at Gln189 (active site), Gln192 (active site), His164 (active site), Arg188 residues. Also, two alkyl bonds at Met165 (active site), Cys145 (active site), and five pi alkyl bonds at His41 (active site), His163 (active site), His164 (active site), Phe181, Pro168 (active site) stabilized the gartanin complex. Maximum non-bonded interaction at the active sites was also observed for robinetin complex

where four hydrogen bonds at Cys44, Asn142, Thr26, Asp187, and two hydrophobic bonds at Met49 and His41 was present.

Discussion

The novel coronavirus namely SARS-CoV-2 has created a pandemic situation due to the high rate of mortality, and no effective drugs or vaccine to treat against SARS-CoV-2 shaped the new global disaster. Although several clinical trials have been undergoing, the drug development methods are time-consuming and costly, there is a need for fast and effective development of active antiviral agents. Conversely, computer-aided drug design may assist the researcher to find the new therapeutic agent against

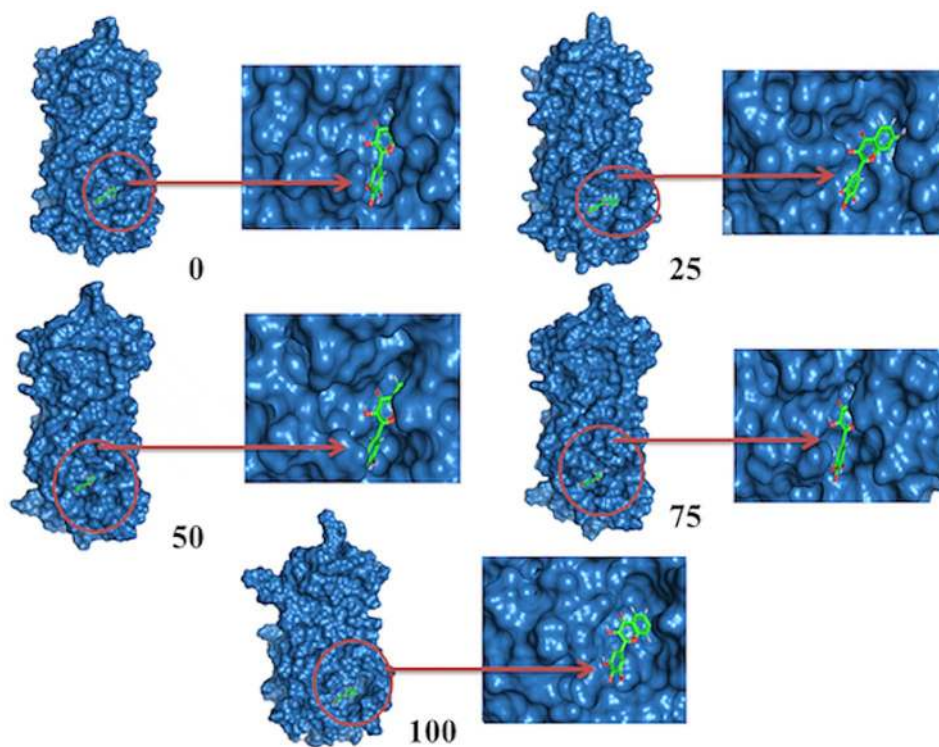


Figure 7. The surface view and the binding pockets of the Gartanin and M^{Pro} complex where 0, 25, 50, 75 and 100 ns snapshots were taken.

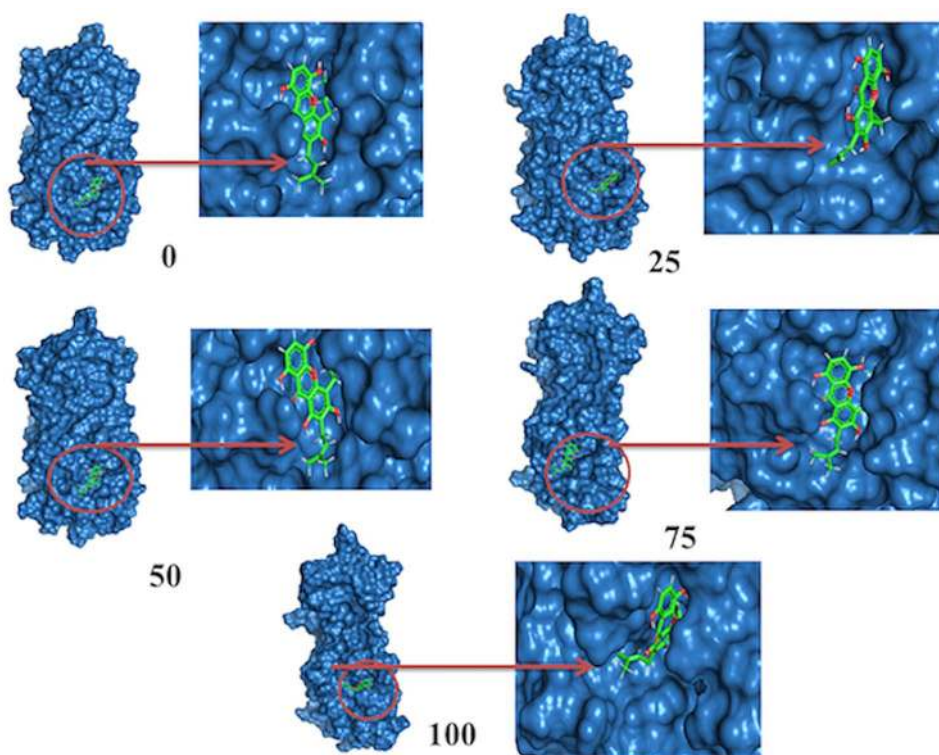


Figure 8. The surface view of the docked Robinetin and M^{Pro} complex by taking 0, 25, 50, 75 and 100 ns snapshots.

SARS-CoV-2 due to its rapid and accurate screening capability from a vast small molecule library [50–52]. Due to having a large impact on the function of SARS-CoV-2, the M^{pro} has become the best target for different therapeutic tactics. It contains three different domain regions; Domain I which covers 1–99 residues, Domain II consists of 100–182 amino acid sequences and Domain III covers 198 to the last residues 303 [11]. It has been observed that the activation through dimerization mechanism through Cys145 and His 41. It is significant that through the drug development technique those catalytic residues would be the best stage for the development of strong inhibitors of M^{pro} [11]. In conjunction with the catalytic sites, there are two more subsites known as S1 and S2, and three more shallow subsites; S3, S4 and S5, where the S1 consist of His163, Glu166, Cys145, Gly143, His172, Phe140 residues, and S2 contains Cys145, His41, and Thr25; whereas the other three subsites consist of Met49, His41, Met165, Glu166 and Gln189 residues [12].

The identification of potent inhibitors from virtual screening workflow allows screening from the diverse large compound library. Additionally, depreciation of the false-positive result in screening modules combinatorial approaches were considered (e.g., HTVS, SP, XP, along with MM-GBSA scoring). These lead compounds identification criteria followed with the addition of binding in the active groove of the targeted protein to explore the possible binding sites in the active points and as well as the interaction dynamics [53–55].

Based on our analysis, we can suggest that the top three screened compounds with better energy interacted with a catalytic residue which is a prerequisite for the inhibition. The first candidate curcumin surrounds curcumin moiety consists of feruloyl chromophores which are joined by a methyl group [56]. The curcumin has chemo-preventive and chemotherapeutic activity [57], anti-inflammation [58], anti-parasite [59], and carcinogenicity suppression [60]. This compound binds with the M^{pro} of SARS-CoV-2 with numerous non-covalent interactions, where it creates one hydrophobic bond at the active cavity (Cys145). Also, it shows seven hydrogen bonds with the active site residues; Gly143, Gln189, Thr190, Pro168, Leu141 and Glu166. Additionally, it also forms two hydrophobic bonds with the targeted M^{pro} at the active region; Met165 and Pro168 [61, 62].

Besides, candidate gartanin is widely known as plant metabolites and antineoplastic agents [63]. The gartanin has activity toward Alzheimer's diseases [64], mTOR pathway as well as anti-cancer agents [65]. This phytochemical compound also showed one hydrogen bond and catalytic amino acid residue from the M^{pro} has hydrophobic bond interaction at His41, one hydrophobic bond, and one pi-Sulfur with the active site residue of Cys145. More significantly, it created six hydrogen bonds in the active part of this protein also; Gly143, Gln189, Asn142. Additionally, two more hydrophobic interactions stabilized the complex by making contacts at Met49 and Met165 [61, 66].

The robinetin has anti-mutagenesis effect [67], anti-tumorigenicity [68], atheroprotective effect [69] in enzymatic and protein assay. The compound robinetin showed one strong hydrogen bond with 3.05 Å at His41 residue along with multiple hydrophobic bonds at the active residue of Cys145. Moreover, multiple hydrogen bonds (Thr26, Asp187 and Met165) at the active groove of the M^{pro} gives the stability of the complex. It also formed two hydrophobic bonds with Met49 correspondingly [61, 70].

Moreover, to understand and endorse the molecular docking study, dynamics simulation was conducted. The RMSD profile from curcumin, gartanin and robinetin did not exceed 2.5 Å as

their average were 1.72, 1.873 1.69 Å, respectively, which specifies their overall integrity. The robinetin and curcumin complex were comparatively more inflexible compared to gartanin as this complex had inflexibility in the middle phase of the simulation. On the other hand, RMSF analysis established that Domain II had strict nature whereas amino acid residues from Domain I and Domain III had more flexibility in the helical and turn region, although almost every residue was fixed. Also, the surface area of these complexes was not altered by surpassing the SASA values too much as their average of curcumin, gartanin and robinetin were 14175.2 Å², 14063.98 Å² and 14161.77 Å², respectively. The hydrogen bonding assessment also aligned with the result of other descriptors from molecular dynamics simulation as they did not over-fluctuate across the simulation trajectory.

Furthermore, superimposition between the docked complex and post-MD docked complex after 100 ns molecular dynamics simulation revealed that both structures had a similar binding position in the active points as the top three complex curcumin, gartanin and robinetin had RMSD value of 1.76, 2.03 and 1.43 Å, respectively (Figure 5). We also took a snapshot (Figures 6–8) from 0, 25, 50, 75 and 100 ns from molecular dynamics simulation trajectory for the top three phytochemicals but no drastic change was observed for their binding pose.

The combinatorial docking and molecular dynamics approach suggest three lead compounds may interfere with the function of the M^{pro} of SARS-CoV-2; however, these plant-derived phytochemicals need to be tested more in the lab to check the efficacy along with inhibitory potential in *in vitro* condition.

Conclusion

In this word, we have employed a computational drug design workflow to recognize potent inhibitors of the M^{pro} from SARS-CoV-2. We have combined the phytochemical dataset consist of over 3000 compounds from Asian plants to investigate their inhibitor potentiality. The virtual screening procedure along with MM-GBSA approaches aids in shortening the list from over 3000 to three potential lead molecules, curcumin, gartanin and robinetin. Furthermore, binding pose and interactions from the docking study were further evaluated through a molecular dynamics simulation study where multiple descriptors from simulation trajectories confirm their stability. We also found that the catalytic residue of the M^{pro}, Cys145 and His41 binds with the drug molecules and their existence was also confirmed in the post-MD structures. However, toxicity and pharmacological estimation of the drug molecules confirms better absorption and metabolism profile along with no toxicity probabilities. Since this study is solely based on multiple computational tools and simulation studies, it requires further evaluation in the lab, and also this study may be helpful for future researchers to work with precise target molecules from an extensive library in search of effective drug development against COVID-19.

Key Points

- The main protease from SARS-CoV-2 can be targeted as an attractive key protein as it has a central role in activating viral replicase through posttranslational modification. The target protein was employed to search for potent inhibitors through virtual screening and molecular dynamics.

- The compound dataset from Asian plants was retrieved by data mining and literature review. These compound lists were used to screen with the combination of molecular docking and MM-GBSA approaches in the virtual screening process.
- The top three drug candidates were further assessed in ADMET filtering where no toxicity and positive pharmacological properties were found.
- The molecular dynamics simulation of the docked complex gives insights into their inflexibility and stability of binding. These potential compounds may be used as a potent drug candidate after further evaluation in the biological lab.

Supplementary data

Supplementary data are available online at *Briefings in Bioinformatics*.

Funding

The authors receive no funding from an external source.

Conflict of Interest

The authors declare no conflict of interest.

References

1. Choudhary S, Malik YS, Tomar S. Identification of SARS-CoV-2 cell entry inhibitors by drug repurposing using in silico structure-based virtual screening approach. *Front Immunol* 2020;**11**:1664.
2. Hui DS, Azhar EI, Madani TA, et al. The continuing 2019-nCoV epidemic threat of novel coronaviruses to global health — the latest 2019 novel coronavirus outbreak in Wuhan, China. *Int J Infect Dis* 2020;**91**:264–6.
3. <https://www.who.int/emergencies/diseases/novel-coronavirus-2019> (1 September 2020, date last accessed).
4. Shang J, Wan Y, Luo C, et al. Cell entry mechanisms of SARS-CoV-2. *Proc Natl Acad Sci USA* 2020;**117**:11727–34.
5. Das S, Sarmah S, Lyndem S, et al. An investigation into the identification of potential inhibitors of SARS-CoV-2 main protease using molecular docking study. *J Biomol Struct Dyn* 2020;1–11. Online publication, <https://doi.org/10.1080/07391102.2020.1763201>.
6. <https://ourworldindata.org/mortality-risk-covid#the-current-case-fatality-rate-of-covid-19> (1 September 2020, date last accessed).
7. Sanche S, Lin YT, Xu C, et al. RESEARCH high contagiousness and rapid spread of severe acute respiratory syndrome coronavirus 2. *Emerg Infect Dis* 2020;**26**:1470–7.
8. Ullrich S, Nitsche C. The SARS-CoV-2 main protease as drug target. *Bioorg Med Chem Lett* 2020;**30**:127377.
9. Rabaan AA, Al-ahmed SH, Haque S, et al. SARS-CoV-2, SARS-CoV, and MERS-CoV: a comparative overview. 2020;**28**(2): 174–84.
10. Neeltje van Doremalen P, Bushmaker T, Infectious (National Institute of Allergy and Diseases), et al. Aerosol and surface stability of SARS-CoV-2 as compared with SARS-CoV-1. *N Engl J Med* 2020;**382**:1564–7.
11. Dai W, Zhang B, Jiang XM, et al. Structure-based design of antiviral drug candidates targeting the SARS-CoV-2 main protease. *Science* 2020;**368**:1331–5.
12. Khan SA, Zia K, Ashraf S, et al. Identification of chymotrypsin-like protease inhibitors of SARS-CoV-2 via integrated computational approach. *J Biomol Struct Dyn* 2020;1–13. Online publication, <https://doi.org/10.1080/07391102.2020.1751298>.
13. Rut W, Groborz K, Zhang L, et al. Substrate specificity profiling of SARS-CoV-2 Mpro protease provides basis for anti-COVID-19 drug design. *bioRxiv* 2020; 2020.03.07.981928.
14. Goyal B, Goyal D. Targeting the dimerization of the main protease of coronaviruses: a potential broad-Spectrum therapeutic strategy. *ACS Comb Sci* 2020. doi: [10.1021/acscomb-sci.0c00058](https://doi.org/10.1021/acscomb-sci.0c00058).
15. Mani JS, Johnson JB, Steel JC, et al. Natural product-derived phytochemicals as potential agents against coronaviruses: a review. *Virus Res* 2020;**284**:297–305.
16. Rajesh KG, Piya PM, Hindol M, Deepu D, et al. Herbal plants and plant preparations as remedial approach for viral diseases. *Virus disease* 2015;**26**(4):225–36.
17. Newman DJ, Cragg GM. Natural products as sources of new drugs from 1981 to 2014. *J Nat Prod* 2016;**79**:629–61.
18. Wan S, Xiang Y, Fang W, et al. Clinical features and treatment of COVID-19 patients in Northeast Chongqing. *J Med Virol* 2020;**92**:797–806.
19. Chen F, Chan KH, Jiang Y, et al. In vitro susceptibility of 10 clinical isolates of SARS coronavirus to selected antiviral compounds. *J Clin Virol* 2004;**31**:69–75.
20. Liu H, Ye F, Sun Q, et al. Scutellaria baicalensis extract and baicalin inhibit replication of SARS-CoV-2 and its 3C-like protease in vitro. 2020. Online publication, doi: <https://doi.org/10.1101/2020.04.10.035824>.
21. Oo A, Rausalu K, Merits A, et al. Deciphering the potential of baicalin as an antiviral agent for chikungunya virus infection. *Antiviral Res* 2018;**150**:101–11.
22. Mahmud S, Parves MR, Riza YM, et al. Exploring the potent inhibitors and binding modes of phospholipase A2 through in silico investigation. *J Biomol Struct Dyn* 2019;1–11. Online publication, <https://doi.org/10.1080/07391102.2019.1680440>.
23. Macalino SJY, Gosu V, Hong S, et al. Role of computer-aided drug design in modern drug discovery. *Arch Pharm Res* 2015;**38**:1686–701.
24. Sethi A, Joshi K, Sasikala K. Molecular docking in modern drug discovery: principles and recent applications. *Drug Discovery and Development-New Advances*. 1–21. doi: [10.5772/intechopen.85991](https://doi.org/10.5772/intechopen.85991).
25. Jin Z, Du X, Xu Y, et al. Structure of Mpro from SARS-CoV-2 and discovery of its inhibitors. *Nature* 2020;**582**: 289–93.
26. Berman HM, Westbrook J, Feng Z, et al. The protein data Bank. *Nucleic Acids Res* 2000;**28**:235–42.
27. Sastry GM, Adzhigirey M, Day T, et al. Protein and ligand preparation: parameters, protocols, and influence on virtual screening enrichments. *J Comput Aided Mol Des* 2013;**27**:221–34.
28. Roos K, Wu C, Damm W, et al. OPLS3e: extending force field coverage for drug-like small molecules. *J Chem Theory Comput* 2019;**15**:1863–74.
29. Kim S, Thiessen PA, Bolton EE, et al. PubChem substance and compound databases. *Nucleic Acids Res* 2016;**44**: D1202–13.
30. Schrödinger, LLC. *LigPrep*. New York, NY: Schrödinger, LLC, 2018-4.

31. Shelley JC, Cholleti A, Frye LL, et al. Epik: a software program for pK prediction and protonation state generation for drug-like molecules. *J Comput Aided Mol Des* 2007;21: 681–91.
32. Riza YM, Parves MR, Tithi FA, et al. Quantum chemical calculation and binding modes of H1R; a combined study of molecular docking and DFT for suggesting therapeutically potent H1R antagonist. *Silico Pharmacol* 2019;7:1.
33. Schrödinger, LLC. QikProp. New York, NY: Schrödinger, LLC, 2019.
34. Lipinski CA. Lead- and drug-like compounds: the rule-of-five revolution. *Drug Discov Today Technol* 2004;1:337–41.
35. Repasky MP, Shelley M, Friesner RA. Flexible ligand docking with glide. *Curr Protoc Bioinformatics* 2007. Online publication, doi: [10.1002/0471250953.bi0812s18](https://doi.org/10.1002/0471250953.bi0812s18).
36. Friesner RA, Murphy RB, Repasky MP, et al. Extra precision glide: docking and scoring incorporating a model of hydrophobic enclosure for protein–ligand complexes. *J Med Chem* 2006;49:6177–96.
37. Mahmud S, Uddin MAR, Zaman M, et al. Molecular docking and dynamics study of natural compound for potential inhibition of main protease of SARS-CoV-2. *J Biomol Struct Dyn* 2020;1–9. Online publication, doi: [10.1080/07391102.2020.1796808](https://doi.org/10.1080/07391102.2020.1796808).
38. Friesner RA, Banks JL, Murphy RB, et al. Glide: a new approach for rapid, accurate docking and scoring. 1. Method and assessment of docking accuracy. *J Med Chem* 2004;47: 1739–49.
39. Chen F, Liu H, Sun H, et al. Assessing the performance of the MM/PBSA and MM/GBSA methods. 6. Capability to predict protein-protein binding free energies and re-rank binding poses generated by protein-protein docking. *Phys Chem Chem Phys* 2016;18:22129–39.
40. Cheng F, Li W, Zhou Y, et al. AdmetSAR: a comprehensive source and free tool for assessment of chemical ADMET properties. *J Chem Inf Model* 2012;52:3099–105.
41. Daina A, Michielin O, Zoete V. SwissADME: a free web tool to evaluate pharmacokinetics, drug-likeness and medicinal chemistry friendliness of small molecules. *Sci Rep* 2017;7:42717.
42. Pires DEV, Blundell TL, Ascher DB. pkCSM: predicting small-molecule pharmacokinetic and toxicity properties using graph-based signatures. *Med. Chem* 2015;58(9):4066–72.
43. Krieger E, Vriend G, Spronk C. YASARA-yet another scientific artificial reality application. 2013. YASARA. org, 993.
44. Case DA, Cerutti DS, Cheatham TE, III, et al. The amber biomolecular simulation programs. 2017. AMBER 2017, University of California, San Francisco.
45. Nam K, Gao J, York DM. An efficient linear-scaling Ewald method for long-range electrostatic interactions in combined QM/MM calculations. *J Chem Theory Comput* 2005;1: 2–13.
46. Krieger E, Nielsen JE, Spronk CAEM, et al. Fast empirical p K a prediction by Ewald summation. *Journal of Molecular Graphics and Modelling* 2006;25:481–6.
47. Krieger E, Vriend G. New ways to boost molecular dynamics simulations. *J Comput Chem* 2015;36:996–1007.
48. Islam MJ, Parves MR, Mahmud S, et al. Assessment of structurally and functionally high-risk nsSNPs impacts on human bone morphogenetic protein receptor type IA (BMPRI1A) by computational approach. *Comput Biol Chem* 2019;80:31–45.
49. Mahmud S, Rahman E, Nain Z, et al. Computational discovery of plant-based inhibitors against human carbonic anhydrase IX and molecular dynamics simulation. *J Biomol Struct Dyn* 2020;1–20. Online publication, doi: [10.1080/07391102.2020.1753579](https://doi.org/10.1080/07391102.2020.1753579).
50. Khan MA, Mahmud S, Alam ASMRU, et al. Comparative molecular investigation of the potential inhibitors against SARS-CoV-2 main protease: a molecular docking study. *J Biomol Struct Dyn* 2020;1–7. Online publication, <https://doi.org/10.1080/07391102.2020.1796813>.
51. Mathpal S, Joshi T, Sharma P, et al. A dynamic simulation study of FDA drug from zinc database against COVID-19 main protease receptor. *J Biomol Struct Dyn* 2020;1–17. Online publication, <https://doi.org/10.1080/07391102.2020.1821785>.
52. Kalhor H, Sadeghi S, Abolhasani H, et al. Repurposing of the approved small molecule drugs in order to inhibit SARS-CoV-2 S protein and human ACE2 interaction through virtual screening approaches. *J Biomol Struct Dyn* 2020;1–16. Online publication, <https://doi.org/10.1080/07391102.2020.1824816>.
53. Beuming T, Lenseink B, Pala D, et al. Docking and virtual screening strategies for GPCR drug discovery. *Methods Mol Biol* 2015;1335:251–76.
54. Kanhed AM, Patel DV, Teli DM, et al. Identification of potential Mpro inhibitors for the treatment of COVID-19 by using systematic virtual screening approach. *Mol Divers* 2020. Online publication, doi: [10.1007/s11030-020-10130-1](https://doi.org/10.1007/s11030-020-10130-1).
55. Pérez-Regidor L, Zariouh M, Ortega L, et al. Virtual screening approaches towards the discovery of toll-like receptor modulators. *Int J Mol Sci* 2016;17:251–76.
56. Nelson KM, Dahlin JL, Bisson J, et al. The essential medicinal chemistry of curcumin. *J Med Chem* 2017;60: 1620–37.
57. Yin HT, Zhang DG, Wu XL, et al. In vivo evaluation of curcumin-loaded nanoparticles in a A549 xenograft mice model. *Asian Pac J Cancer Prev* 2013;14:409–12.
58. Yan D, Geusz ME, Jamasbi RJ. Properties of Lewis lung carcinoma cells surviving curcumin toxicity. *J Cancer* 2012;3:32–41.
59. Said DE, ElSamad LM, Gohar YM. Validity of silver, chitosan, and curcumin nanoparticles as anti-giardia agents. *Parasitol Res* 2012;111:545–54.
60. Mach CM, Mathew L, Mosley SA, et al. Determination of minimum effective dose and optimal dosing schedule for liposomal curcumin in a xenograft human pancreatic cancer model. *Anticancer Res* 2009;29:1895–9.
61. Kumar Y, Singh H, Patel CN. In silico prediction of potential inhibitors for the main protease of SARS-CoV-2 using molecular docking and dynamics simulation based drug-repurposing. *J Infect Public Health* 2020;13: 1210–23.
62. Mohammad T, Shamsi A, Anwar S, et al. Identification of high-affinity inhibitors of SARS-CoV-2 main protease: towards the development of effective COVID-19 therapy. *Virus Res* 2020;288:198102.
63. Li G, Petiwala SM, Yan M, et al. Gartanin, an isoprenylated xanthone from the mangosteen fruit (*Garcinia mangostana*), is an androgen receptor degradation enhancer. *Mol Nutr Food Res* 2016;60:1458–69.
64. Wang SN, Li Q, Jing MH, et al. Natural Xanthones from *Garcinia mangostana* with multifunctional activities for the therapy of Alzheimer's disease. *Neurochem Res* 2016;41:1806–17.
65. Liu Z, Antalek M, Nguyen L, et al. The effect of gartanin, a naturally occurring xanthone in mangosteen juice, on the mTOR pathway, autophagy, apoptosis, and the growth of human urinary bladder cancer cell lines. *Nutr Cancer* 2013;65:68–77.

66. Mpiana PT, Ngbolua K-t-N, Tshibangu DST, et al. Identification of potential inhibitors of SARS-CoV-2 main protease from Aloe vera compounds: a molecular docking study. *Chem Phys Lett* 2020;**754**:137751.
67. Birt DF, Walker B, Tibbels MG, et al. Anti-mutagenesis and anti-promotion by apigenin, robinetin and indole-3-carbinol. *Carcinogenesis* 1986;**7**:959–63.
68. Chang RL, Huang MT, Wood AW, et al. Effect of ellagic acid and hydroxylated flavonoids on the tumorigenicity of benzo[a]pyrene and (\pm)-7 β , 8 α -dihydroxy-9 α , 10 α -epoxy-7,8,9,10-tetrahydrobenzo[a]pyrene on mouse skin and in the newborn mouse. *Carcinogenesis* 1985;**6**:1127–33.
69. Kyaw M, Yoshizumi M, Tsuchiya K, et al. Atheroprotective effects of antioxidants through inhibition of mitogen-activated protein kinases. *Acta Pharmacol Sin* 2004;**25**:977–85.
70. Zhang L, Lin D, Sun X, et al. Crystal structure of SARS-CoV-2 main protease provides a basis for design of improved α -ketoamide inhibitors. *Science* 2020;**368**:409–12.